Supporting Information for

The Gore-Tex® Effect in Externally Hydrophobic Metal-Organic Frameworks

Kaleb L. Miller,[b] Rijia Lin,[c] Jingwei Hou,[c] Cameron J. Kepert,*[b] Deanna M. D'Alessandro,*[ab] Marcello B. Solomon*[ab]

[a] School of Chemical and Biological Engineering, The University of Sydney, New South Wales 2006, Australia.
[b] School of Chemistry, The University of Sydney, New South Wales 2006, Australia.
[c] School of Chemical Engineering, The University of Queensland, Queensland 4072, Australia

* *Corresponding Authors:* cameron.kepert@sydney.edu.au deanna.dalessandro@sydney.edu.au; marcello.solomon@sydney.edu.au

Table of Contents

Materials and Methods

Materials

Unless otherwise stated, all reagents and solvents employed were commercially available and used as received without further purification.

Methods

Powder X-ray Diffraction (PXRD): PXRD Diffractograms were recorded using a PANalytical X'Pert Pro Diffractometer equipped with a PIXcel3D detector. The diffractometer was operated at 45 kV and 40 mA producing Cu-K_α radiation (λ = 1.5406 Å) for diffraction experiments. Typically, the dried sample (~ 10 mg) was ground into a fine powder and loaded onto a silicon zero diffraction plate. Diffraction patterns were collected over 2θ = 5-50° with a scan rate of 0.03125° s^{-1}.

Fourier-Transformed Infrared (FT-IR) Spectroscopy: FT-IR spectra were collected on a Bruker VERTEX 80v vacuum FT-IR spectrometer. The sample (~ 1 mg) was finely ground prior to measurement. Each spectrum consisted of 64 scans that were collected over the range 400-4000 cm^{-1} with a resolution of 2 cm^{-1}

Scanning Electron Microscopy (SEM): SEM images were taken at The Australian Centre of Microscopy and Microanalysis (ACMM) using a JEOL JSM-7600F field emission scanning electron microscope. It is equipped with a motorised x-y-z-tiltrotate stage, providing the following movements: x = y = 150 mm (motorised); z = 65 mm (motorised); Tilt +70 degrees to –5 degrees (motorised); Source: Field emission 3 gun assembly with Schottky emitter source. Voltage: 200 V to 30 kV. Samples were coated with a 10 nm gold layer to enhance conductivity with a Safematic CCU-010 HV high vacuum sputter coater.

Thermogravimetric Analysis (TGA):

<u>*Thermal Decomposition Studies:*</u> TGA data were recorded under air (20 mL min^{-1}) on a TA Discovery TGA instrument. The sample (~10 mg) was loaded onto a platinum pan. Each sample was heated to 700 °C at a ramp rate of 10 °C min^{-1}.

<u>*Cycling:*</u> TGA data were collected on a Mettler Toledo TGA/SDTA851e. The sample (~10 mg) was loaded into a quartz crucible for analysis. Data were collected under both dry and humid conditions.

For dry cycling, the sample was first activated by heating the sample to 140 °C at a ramp rate of 10 °C min^{-1}, where it was held for 30 min. The sample was cooled at 2 °C min^{-1} to 30 °C. The program was cycled four times between 30 and 120 °C, with a heating rate of 10 °C min^{-1} under N_2 (50 mL min^{-1}), and a cooling rate of 2 °C min^{-1} under CO_2 (50 mL min^{-1}).

For humid cycling, a humid gas stream was obtained by flowing cylinder gas (either N_2 or instrument air – 50 mL min^{-1}) through a custom designed double bubbler containing a saturated solution of $MgCl_2$ (~ 30% Relative Humidity[1]), prior to being flowed across the sample. The sample was first activated by heating the sample under dry N_2 (50 mL min^{-1}) to 140 °C at a ramp rate of 10 °C min^{-1}, where it was held for 30 min. The sample was cooled at 2 °C min^{-1} to 30 °C. The program was then cycled under humid air (50 mL min^{-1}) four times between 30 and 120 °C, with a heating rate of 10 °C min^{-1} and a cooling rate of 2 °C min^{-1}.

Gas Adsorption: Gas adsorption experiments (0 to ~1200 mbar) were performed on a Micromeritics 3Flex Surface Area and Pore Size Analyzer. Samples were first degassed on a Smart VacPrep Instrument at 110 °C for 20 h. Brunauer-Emmett-Teller (BET)[2] surface areas of the materials were first determined from the N_2 adsorption isotherms collected at 77 K with ultra-high-purity grade N_2. BET Pore size distribution was determined from the N_2 isotherm using the Micromeritics suite with a Density Functional Theory model to fit the data.

Low-pressure CO_2 measurements were performed at 288 K, 298 K and 308 K using ultra-high-purity grade CO_2. A Julabo temperature controller was used to maintain a constant temperature in the recirculating bath for the duration of the experiment.

Water Vapour Adsorption: Water vapour experiments (0 to ~ 30 mbar) were performed on a Micromeritics 3Flex Surface Area and Pore Size Analyzer fitted with vapour option. Water was first degassed on a Schlenk line through three freeze-pump-thaw cycles. The partially degassed water (~ 17 mL) was then loaded into the vapour canister. Freeze-pump-thaw cycles were continued *in situ* on the 3Flex until the vapour pressure of water at room temperature was reached (~ 30 mbar).[3]

Breakthrough: Real time CO_2 separation from N_2 for each composite material was examined *via* fixed-bed column breakthrough experiments, using a binary CO_2/N_2 mixture (50:50) and a custom made rig. Samples (~ 350 mg) were filled into a column (4 mm ID) and were activated at 120 °C under vacuum overnight. The system was purged under helium flow for 30 min, prior to breakthrough

experiments. Then 2.2 mL min^{-1} of A CO_2/N_2 mixture (50:50) was introduced through the sample column at a flow rate of 2.2 mL min^{-1} and the gas outlets from the sample columns were monitored using a gas chromatograph (SHIMAZU GC-2014).

Water Contact Angle Experiments: Water contact angle measurements were performed by placing a droplet of water (~1 μL) onto a compacted surface of the MOF using a hypodermic needle and syringe. The surface was prepared by pressing a sample of the hydrophobic MOF composite material (~10 mg) onto a glass slide to create a flat, even surface. An image of the droplet on the surface was taken with a digital camera and the image processed with ImageJ,[4] with the water contact angle plugin. The droplet shape was fit using both ellipsoidal and circular fits to find the average angle of contact.

Synthesis of UiO-66-NH_2 and its Hydrophobic Derivatives

Synthesis of UiO-66-NH_2: UiO-66-NH_2 was synthesised *via* a solvothermal route according to a reported literature procedure.[5] 2-Aminoterepthalic acid (0.720 g, 3.997 mmol), zirconium chloride (1.288 g, 3.972 mmol), and hydrochloric acid (8 mL, 32%, 10 M) were dissolved in *N*,*N*'-dimethylformamide (DMF) (100 mL). The reaction solution was sealed in a Teflon lined steel autoclave and heated at 120 °C for 24 hours, then allowed to cool to room temperature. The product was washed with DMF (3 × 20 mL) then ethanol (3 × 40 mL), and dried at 100 °C to afford a pale-yellow powder (1.100 g). The characterisation matched that reported in the literature.[5]

Strategy One: Synthesis of Hydrophobic UiO-66-NH_2 *via* Enteric Polymer Coating: The commercially available Eudragit RL enteric polymer[6] (Evonik Industries) was chosen as the candidate enteric coating. Eudragit RL was dissolved in a solution of methanol and chloroform (1:1, 10 mL) at 1,2 and 4 wt/v%. Finely ground UiO-66-NH_2 powder (100 mg) was suspended in the coating solutions (5 mL), which were agitated for 30 minutes *via* a lab shaker to facilitate the coating process. The coated UiO-66-NH_2 was collected *via* centrifugation and dried in an oven at 80 °C for 24 hours to yield the UiO-66-NH_2/Eudragit RL (UiO-66-NH_2/Eu) composite material.

Strategy Two: Synthesis of Hydrophobic UiO-66-NH_2 *via* Long Chained Alkane Surface Modification: Palmitic acid ($C_{16}H_{32}O_2$) was chosen as the candidate long chained alkane. Palmitic acid (100 mg) was dissolved in diethyl ether (5 mL). Finely ground UiO-66-NH_2 powder (100 mg) was suspended in the coating solution (5 mL), which was heated at 30 °C for 30 minutes, 1 hour, 3 hours or 24 hours. The product was then collected *via* centrifugation, washed with ethanol (3 × 20 mL) and dried at 80 °C for 24 hours to yield the UiO-66-NH_2/palmitic acid (UiO-66-NH_2/PA) composite material.

Strategy Three: Synthesis of Hydrophobic UiO-66-NH_2 *via* Organosilicon Infiltration: DOWSIL™ 1-2577 Conformal Coating (DOW Chemical Company) was chosen as the candidate organosilicon. A solution of coating was prepared by dissolving the coating (40 mg) in hexane (5 mL). Finely ground UiO-66-NH_2 powder (100 mg) was suspended in the coating solution (1 mL), which was agitated *via* a lab shaker for 1 hour to facilitate the coating process. The suspension was then dried under vacuum for 12 hours to yield the UiO-66-NH_2/DOWSIL 1-2577 (UiO-66-NH_2/DC) composite material.

Strategy Four: Synthesis of Hydrophobic UiO-66-NH_2 *via* Secondary Building Unit Functionalisation: Phenylsilane was chosen as the candidate grafting agent. Under an inert environment, finely ground UiO-66-NH_2 (117 mg) and Cs_2CO_3 (32.4 mg, 0.992 mmol) were added to a Schlenk tube and degassed with nitrogen three times. A solution of phenylsilane was prepared by mixing anhydrous acetonitrile (2 mL) with phenylsilane (0.37 mL, 3.00 mmol) in an inert environment. This solution was injected into the reaction vessel containing the UiO-66-NH_2/Cs_2CO_3 mixture. The tube was then purged with CO_2 for 20 minutes and sealed under a CO_2 atmosphere to promote the reaction. The reaction was heated at 80 °C with stirring for 24 hours. The resulting powder was washed with ethanol (20 mL) and dried under vacuum to yield the UiO-66-NH_2/phenylsilane (UiO-66-NH_2/ph) composite material.

Characterisation of UiO-66-NH$_2$

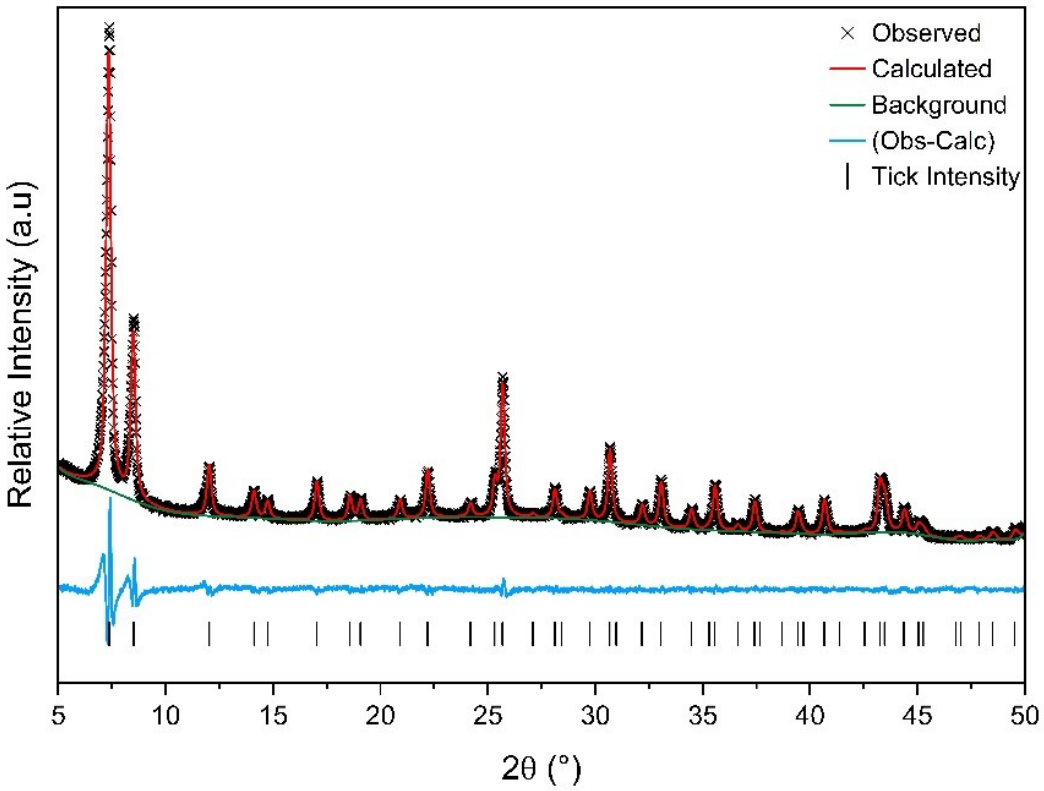

Figure S1: PXRD of UiO-66-NH$_2$ (black), fit with Le Bail model (red), background shown in green, and the difference shown in blue.

Table S1: Le Bail parameters for UiO-66-NH$_2$

a (Å)	20.80912
b (Å)	20.80912
c (Å)	20.80912
ß (°)	90
V (Å^3)	9010.755
Space Group	F*m*-3*m*
R_p	2.105
R_{wp}	4.562
Goodness of Fit	2.710

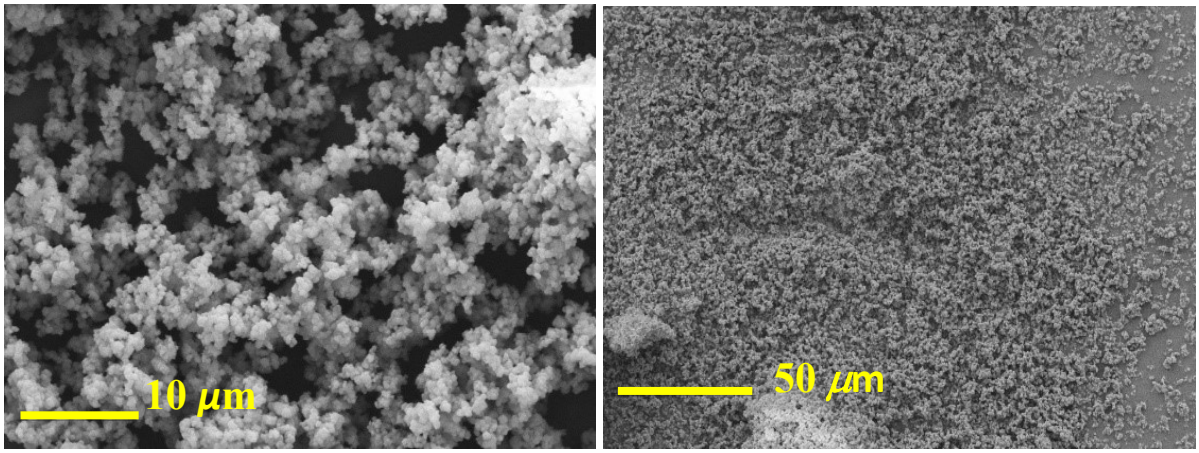

(a) 2400× zoom **(b)** 540× zoom

Figure S2: SEM images of as-synthesised UiO-66-NH_2 at **(a)** 2400× zoom and **(b)** 540× zoom.

Strategy One Optimisation

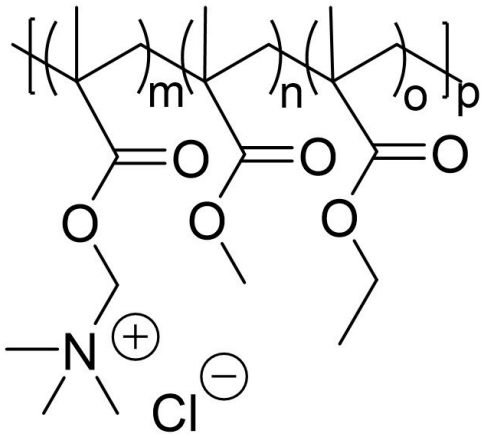

Figure S3: The structure of Eudragit RL® copolymer.

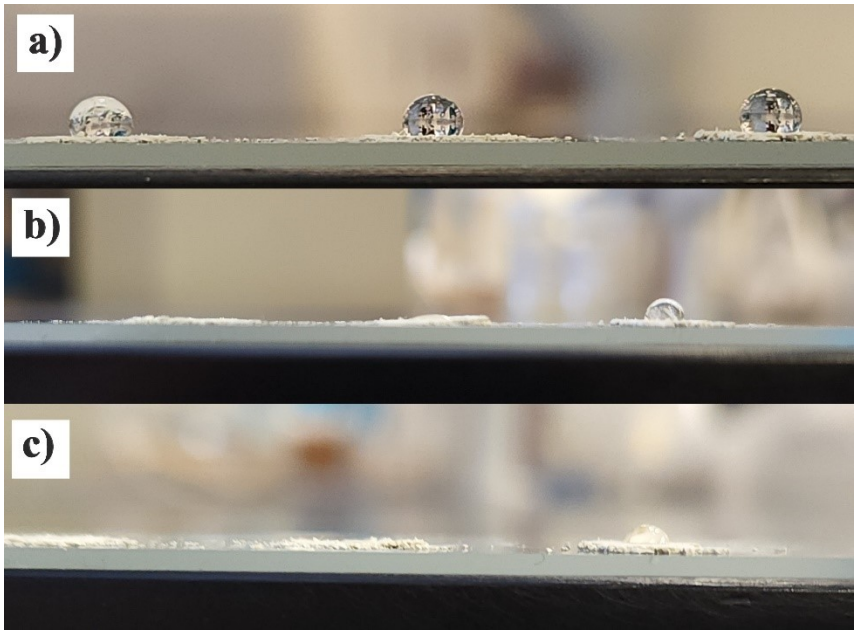

Figure S4: Water contact angle images on UiO-66-NH_2/Eu1 (left), UiO-66-NH_2/Eu2 (middle) and UiO-66-NH_2/Eu5 (right) at **(a)** time of initial exposure, **(b)** 30 minutes following exposure and **(c)** 1 hour following exposure.

Structural characterisation of the post-synthetically modified UiO-66-NH_2 reveals the successful incorporation of Eudragit RL®. PXRD data shows preservation of the UiO-66-NH_2 structure (Figure S5), while SEM data indicates no major morphological differences prior to and after the coating process (Figure S6). Particle conglomeration is observed after coating. FT-IR spectroscopy indicates the presence of Eudragit RL® in the framework. The appearance of spectroscopic features at 1200 cm^{-1} and 1730 cm^{-1} are likely due to C-H and C=O vibrational modes present in the enteric coating side chains (Figure S7). The composite material was characterised thermally using thermogravimetric analysis (Figure S8). Increasing the concentration of enteric coating does not impact the onset temperature for framework decomposition. Finally, the amount of Eudragit RL® in the composite material was confirmed by recovering the used supernatant following reaction with the pristine UiO-66-NH_2 (Table S2).

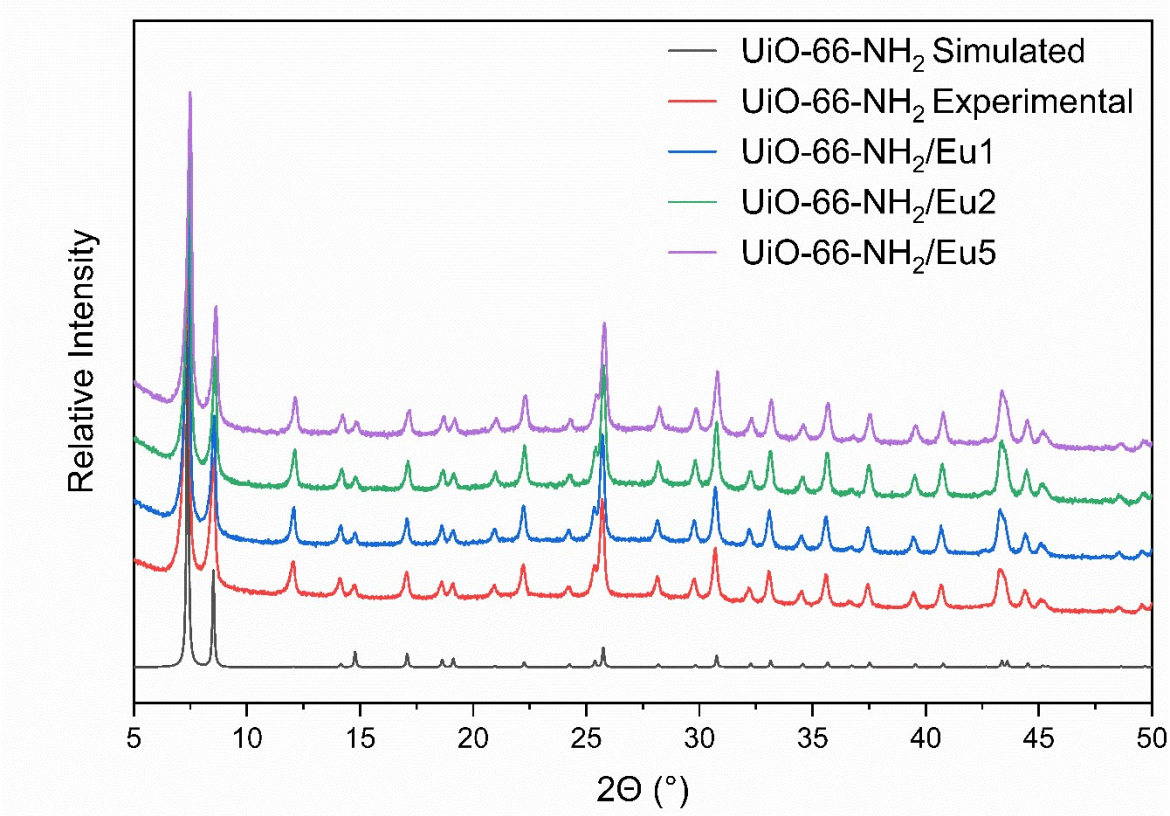

Figure S5: PXRD of UiO-66-NH_2 simulated (black) and experimental (red). The samples were coated in a solution of Eudragit RL® (1 wt% - blue, 2 wt% - green and 5 wt% - purple).

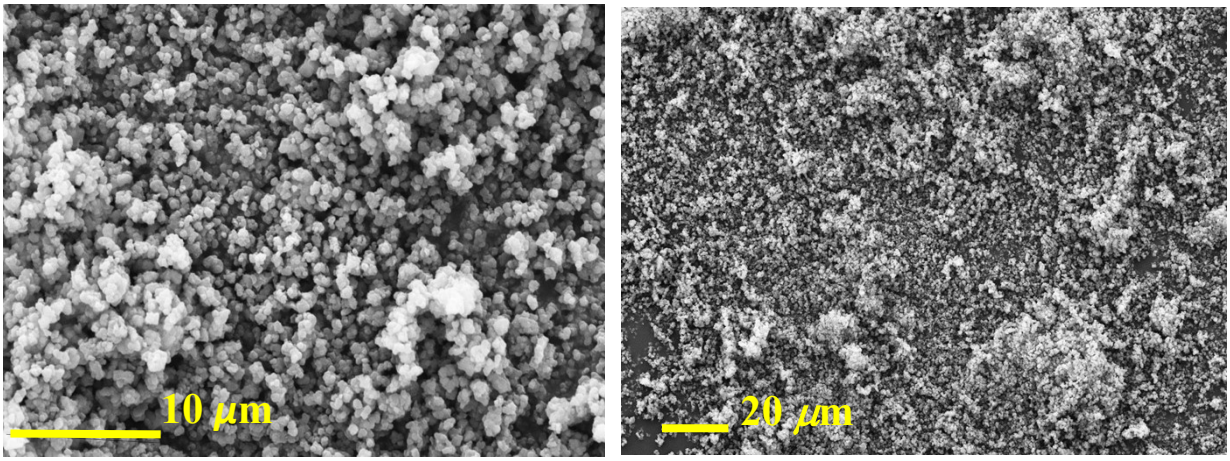

(a) 3000× zoom **(b)** 650× zoom

Figure S6: SEM images of as-synthesised UiO-66-NH_2/Eu at **(a)** 3000× zoom and **(b)** 650× zoom.

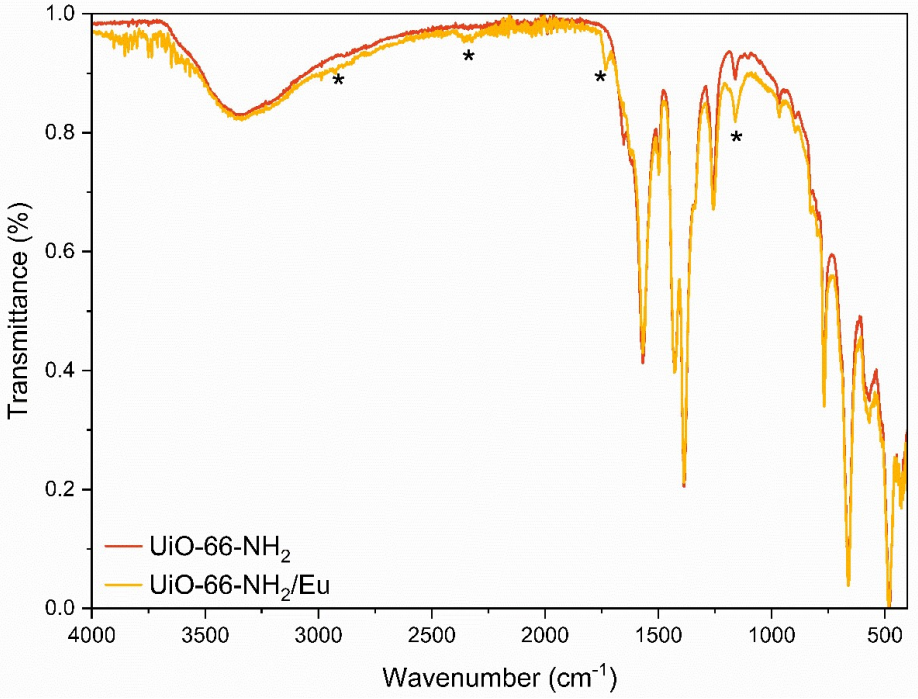

Figure S7: FT-IR spectra of UiO-66-NH_2/Eu (yellow) compared with the as-synthesised UiO-66-NH_2 (red). Changes in spectroscopic features are highlighted with an *.

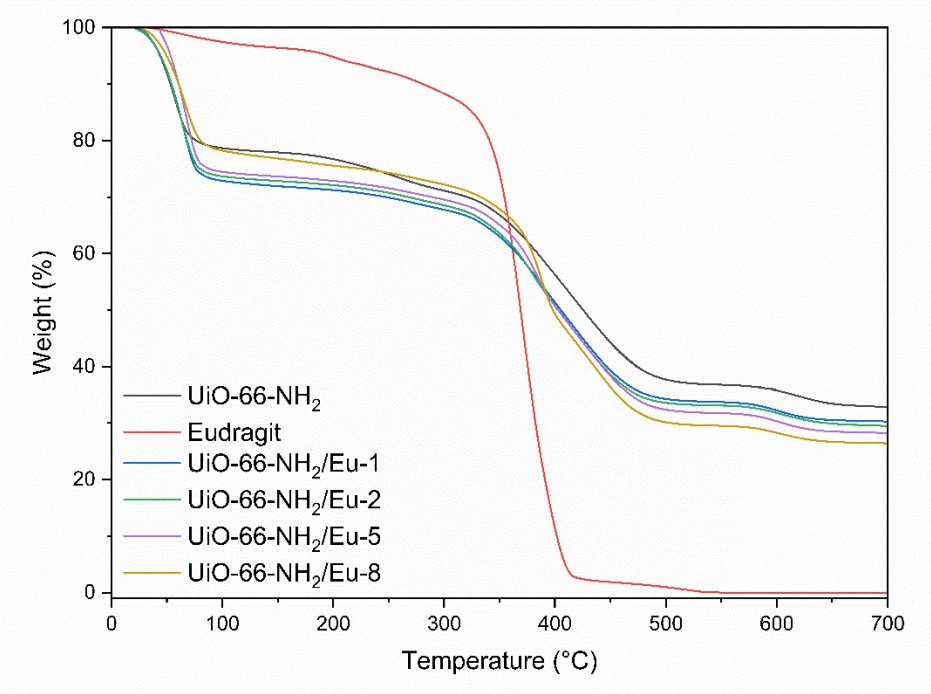

Figure S8: TGA decomposition curves of UiO-66-NH_2/Eu after coating with a solution of 1% (blue), 2% (green) and 5 wt% (purple). Decomposition curves were compared to as-synthesised UiO-66-NH_2 (black) and Eudragit RL ® (red).

Table S2: Calculation of Eudragit RL ® in UiO-66-NH_2/Eu.

Mass of Eu in Coating Solution (mg)	200
Mass of Recovered Eu (mg)	197
Mass of Eu Coating on MOF (mg)	3
Coating of Eu (% w/w)	**3**

Strategy Two Optimisation

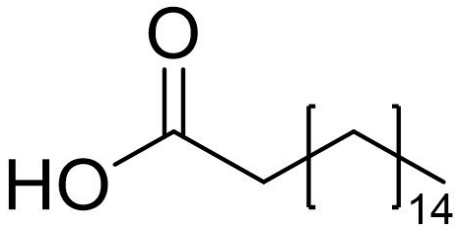

Figure S9: The structure of palmitic acid (hexadecenoic acid).

The inclusion of palmitic acid was confirmed through the structural characterisation of the composite material. PXRD data reveals the preservation of the UiO-66-NH_2 structure, with a degree of peak broadening and a slight loss of crystallinity of the composite structure (Figure S10). Peak broadening may be caused by the decrease in long-range order in the composite material resulting from the long, disordered, amorphous polymer chains being tethered to the MOF. No significant morphological differences can be observed in the SEM images of the composite (Figure S11); however, greater surface charging of the material with the same conductive coating indicates the material has become less conductive.[7] This could be in part due to the insulating properties of long chained alkanes. FT-IR spectroscopy data further confirm the functionalisation of UiO-66-NH_2 with palmitic acid (Figure S12). The emergence of new features at 2900 cm^{-1} and 1000 cm^{-1} can be attributed to the respective C-H and C-O stretching modes of the palmitic acid. The composite material was analysed thermogravimetrically (Figure S13, ESI). Incorporation of palmitic acid into the MOF increases the onset decomposition of the palmitic acid from 200 °C to 350 °C. The onset decomposition of the composite is only 50 °C lower than that observed in the as-synthesised UiO-66-NH_2. Finally, the amount of palmitic acid in the composite material was determined by recovering the used supernatant following reaction with UiO-66-NH_2 (Table S3).

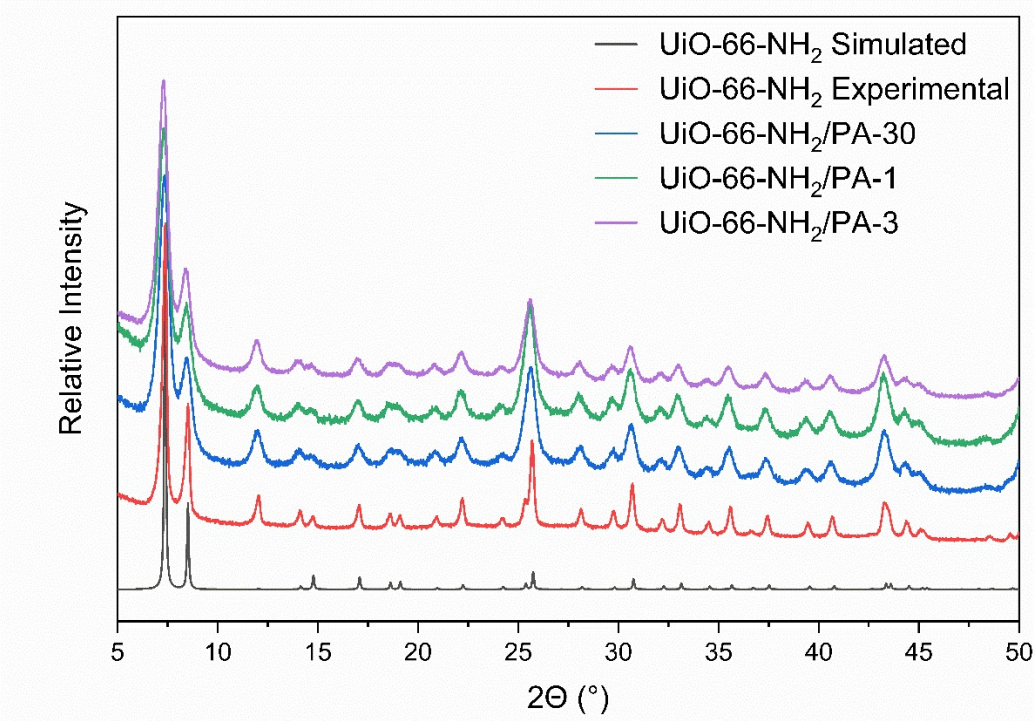

Figure S10: PXRD of UiO-66-NH_2 simulated (black) and as synthesised (red). PXRD was measured after modification with palmitic acid for 30 minutes (blue), 1 hour (green) and 3 hours (purple).

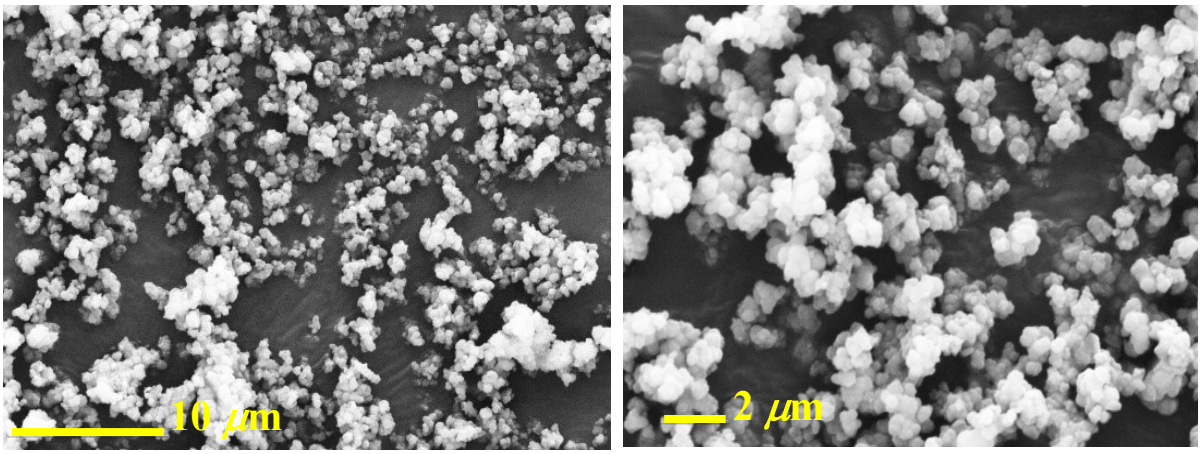

(a) 3000× zoom **(b)** 6600× zoom

Figure S11: SEM images of as-synthesised UiO-66-NH_2/PA at **(a)** 3000× zoom and **(b)** 6600× zoom.

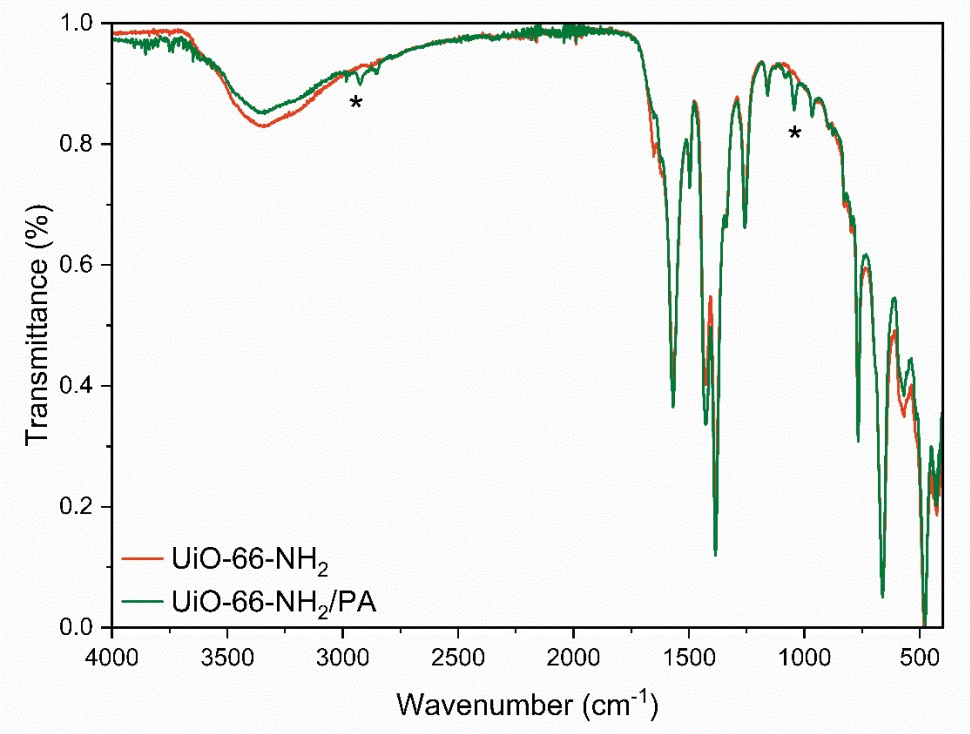

Figure S12: FT-IR spectroscopy of as-synthesised UiO-66-NH_2 (red) and UiO-66-NH_2/PA (green). The appearance of new spectroscopic features are highlighted with an *.

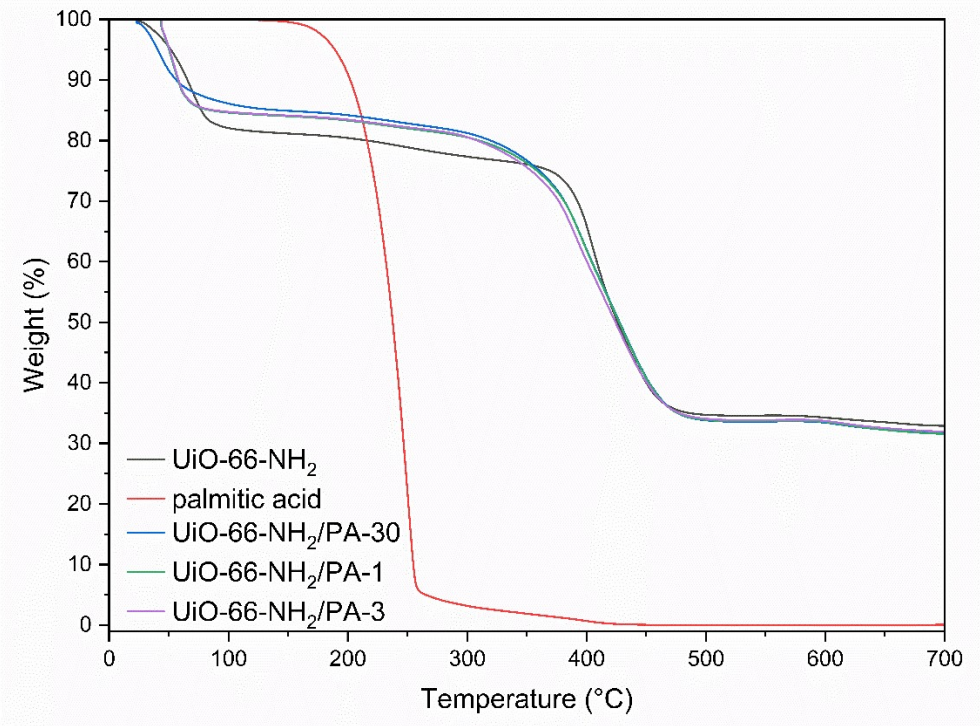

Figure S13: TGA decomposition curves of UiO-66-NH_2 (black), free palmitic acid (red) and UiO-66-NH_2 (blue).

Table S3: Calculation of palmitic acid in UiO-66-NH_2/PA.

Mass of PA in Coating Solution (mg)	100
Mass of Recovered PA (mg)	98
Mass of Eu Coating on MOF (mg)	2
Coating of Eu (% w/w)	**2**

Strategy Three Optimisation

(a) **(b)**

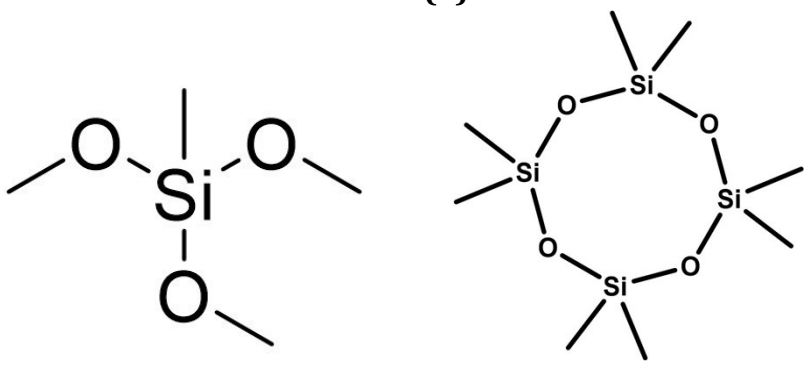

Figure S14: The active hydrophobic agents in DOWSIL™ 1-2577 Conformal (DC) coating: **(a)** methyltrimethoxysilane and **(b)** octamethyl cyclotetrasiloxane.

PXRD indicates that the composite MOF retains its structure after being coated by the organosilicon coating, consistent with a predominately surface-based coating process (Figure S15).[8] Other than increased particle aggregation as a result from the sticky nature of DC, SEM images do not display any significant differences between pristine and coated MOF (Figure S16). FT-IR spectroscopy data further confirms the presence of organosilicon, with the emergence of peaks around 900-1100 cm^{-1}, corresponding to O-Si-O stretches in the methylytrimethoxysilane and octamethyl cyclotetrasiloxane, respectively (Figure S17).[9] Finally, the incorporation of the organosilicon coating was observed in the Thermogravimetric Analysis (TGA) (Figure S18). The TGA of UiO-66-NH_2/DC demonstrated consistently lower mass loss over the experiment and did not affect the onset decomposition of the MOF. This is likely due to the presence of the non-volatile, more stable organosilicon. A smaller solvent loss in the initial weight loss step is likely due to the reduced pore volume of the coated material.

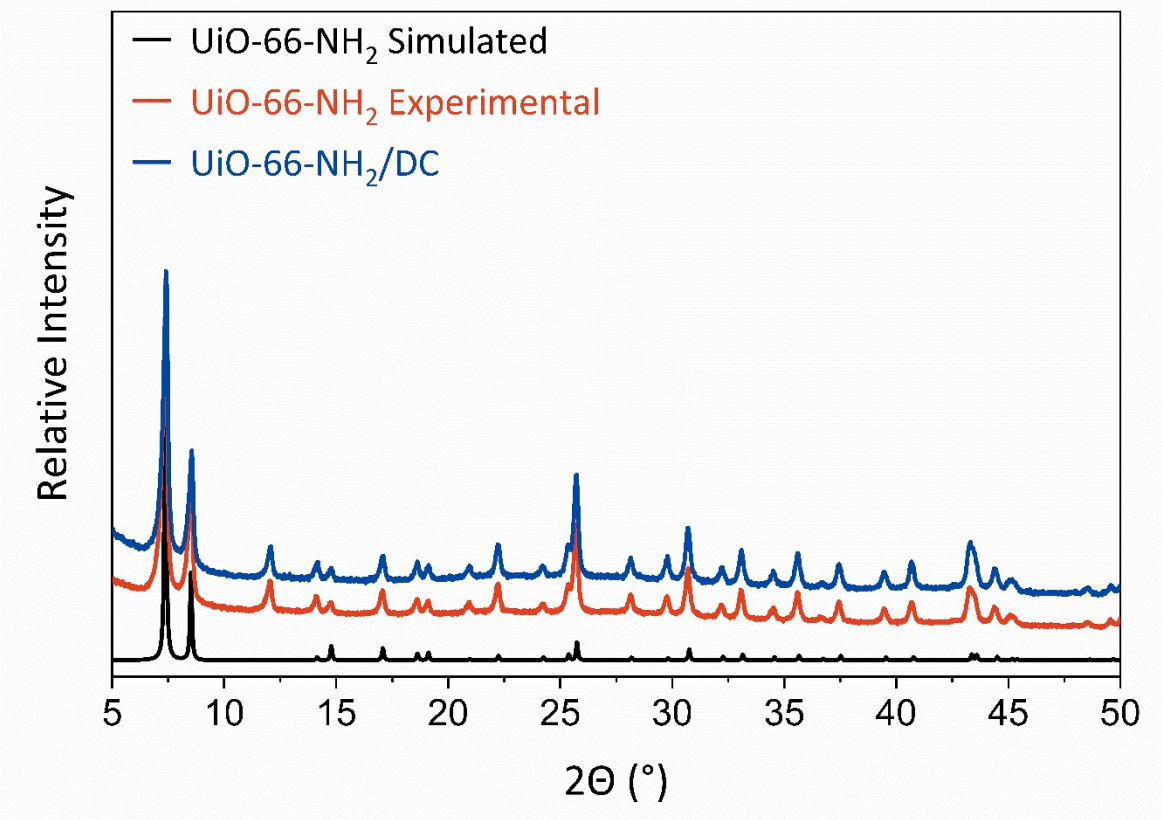

Figure S15: PXRD of simulated (black) and as-synthesised (red) UiO-66-NH_2 and UiO-66-NH_2/DC (blue).

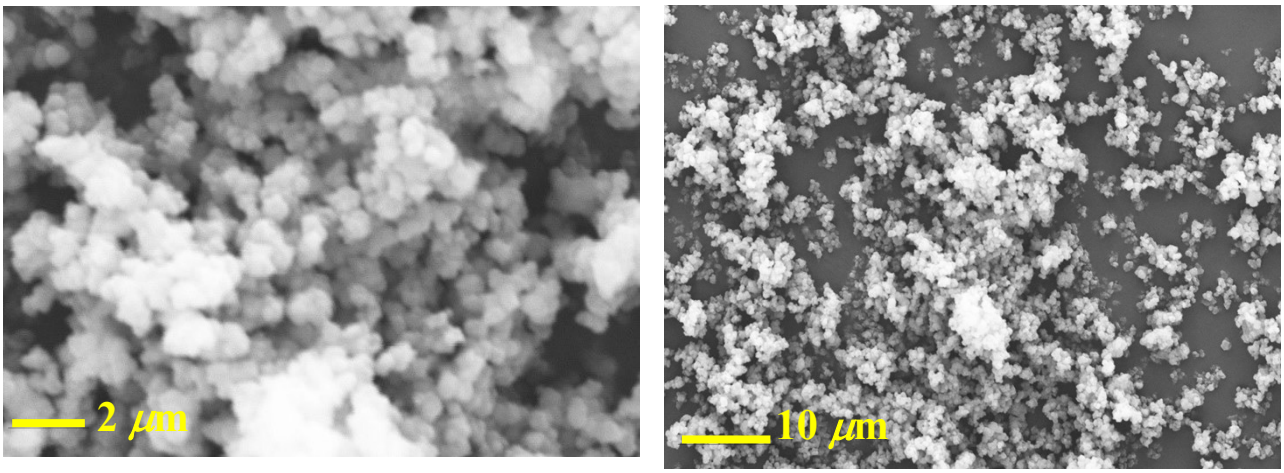

(a) 7000× zoom **(b)** 1700× zoom

Figure S16: SEM images of as-synthesised UiO-66-NH_2/DC at **(a)** 7000× zoom and **(b)** 1700× zoom.

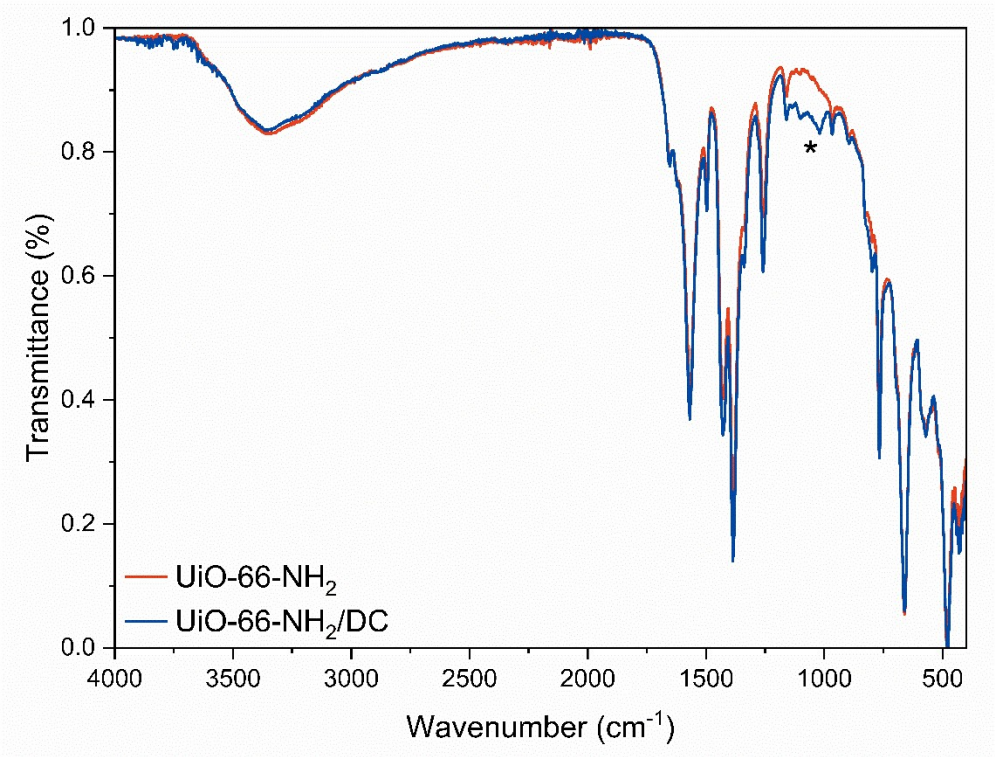

Figure S17: FT-IR of UiO-66-NH_2/DC (blue) and UiO-66-NH_2 (red). The appearance of new spectroscopic features are highlighted with an *.

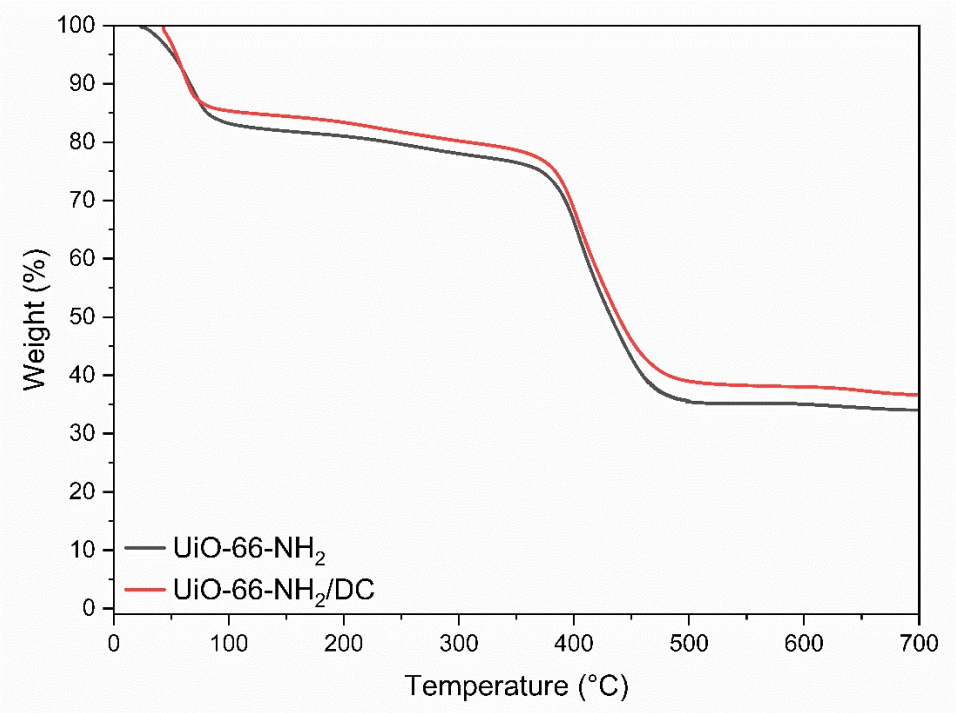

Figure S18: TGA decomposition curves of UiO-66-NH_2 (black) and UiO-66-NH_2/DC (red).

Strategy Four Optimisation

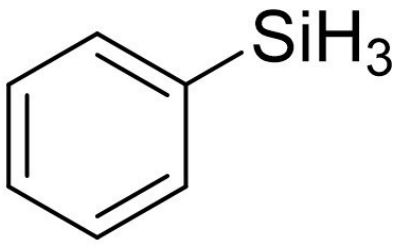

Figure S19: The structure of phenylsilane.

Preservation of the structure of the grafted MOF is confirmed by PXRD (Figure S20), which is consistent with previous studies.[10, 11] Although the crystallinity was preserved, SEM reveals very significant morphological changes (Figure S21). The particle size and roughness of the composite material increased, which may occur from a self-polymerisation between phenylsilane moieties.[12] Significant changes in the physical structure of the composite are found in FT-IR spectroscopy (Figure S22). New spectroscopic features occur at 1134 and 1028 cm^{-1}, which correspond to new Si-O bonds formed between the phenylsilane and the SBU.[10] Concurrently, there is a reduction in the intensity of the broad feature at 3300 cm^{-1}, attributable to the conversion of -OH groups on the UiO-66-NH_2 SBU where phenylsilane is grafted.[10] TGA reveals significant changes in the decomposition profile of the composite and the parent MOF (Figure S23). The initial surface solvent loss of the composite material is smaller and occurs at a higher onset temperature compared to the MOF, attributable to the presence of the organosilicon in the pores and on the surface. The onset decomposition temperature of the composite is at 350 °C, which is lower than the onset for pristine UiO-66-NH_2.

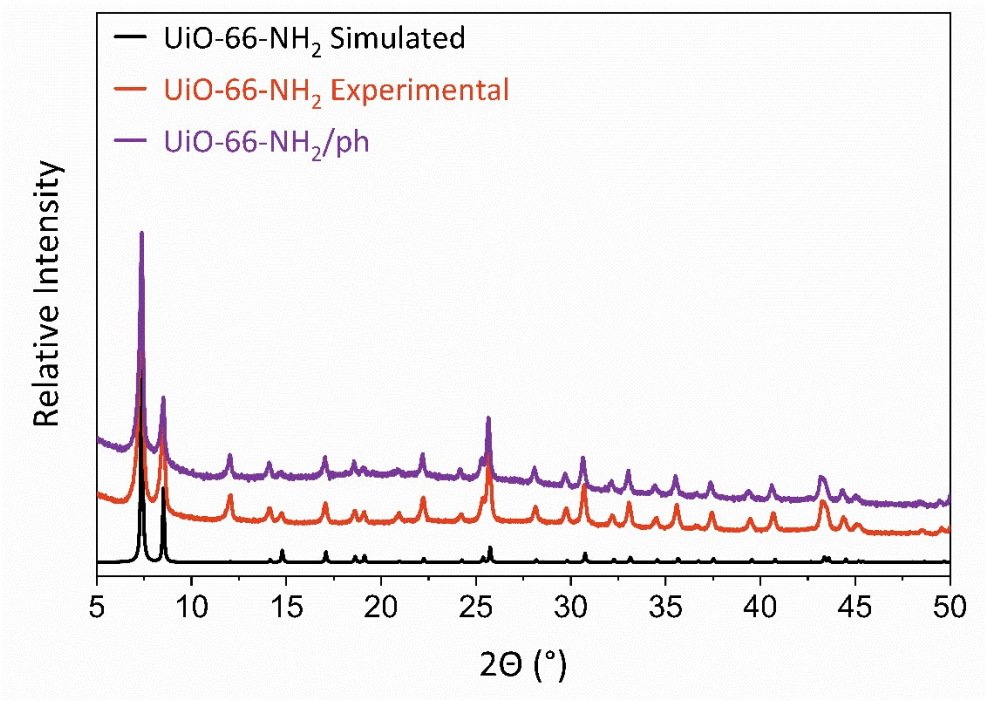

Figure S20: PXRD patterns of simulated (black) and as-synthesised (red) UiO-66-NH_2, and UiO-66-NH_2/ph (purple).

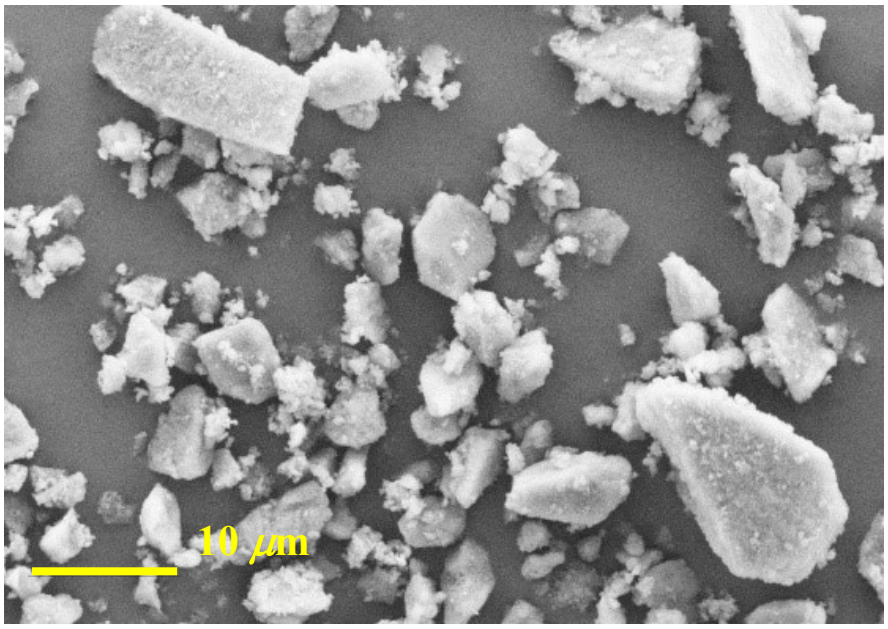

2000× zoom

Figure S21: SEM images of as-synthesised UiO-66-NH_2/ph at 2000× zoom.

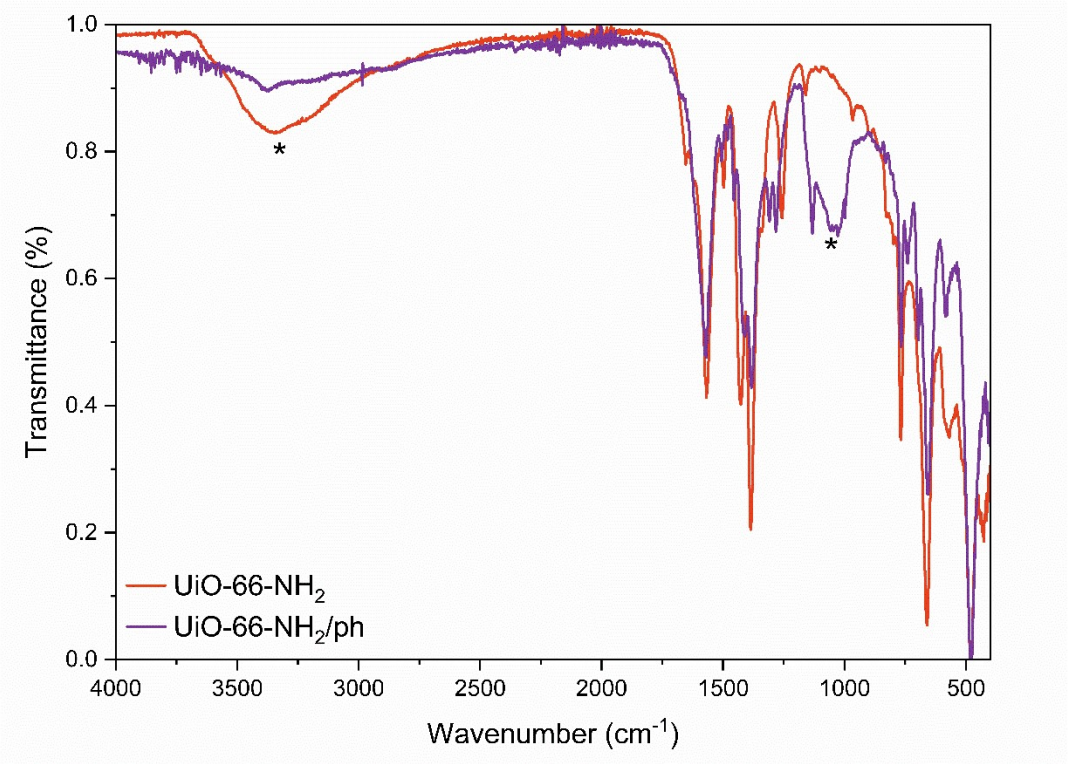

Figure S22: FT-IR of UiO-66-NH_2/ph (purple) and UiO-66-NH_2 (red). The appearance of new spectroscopic features are highlighted with an *.

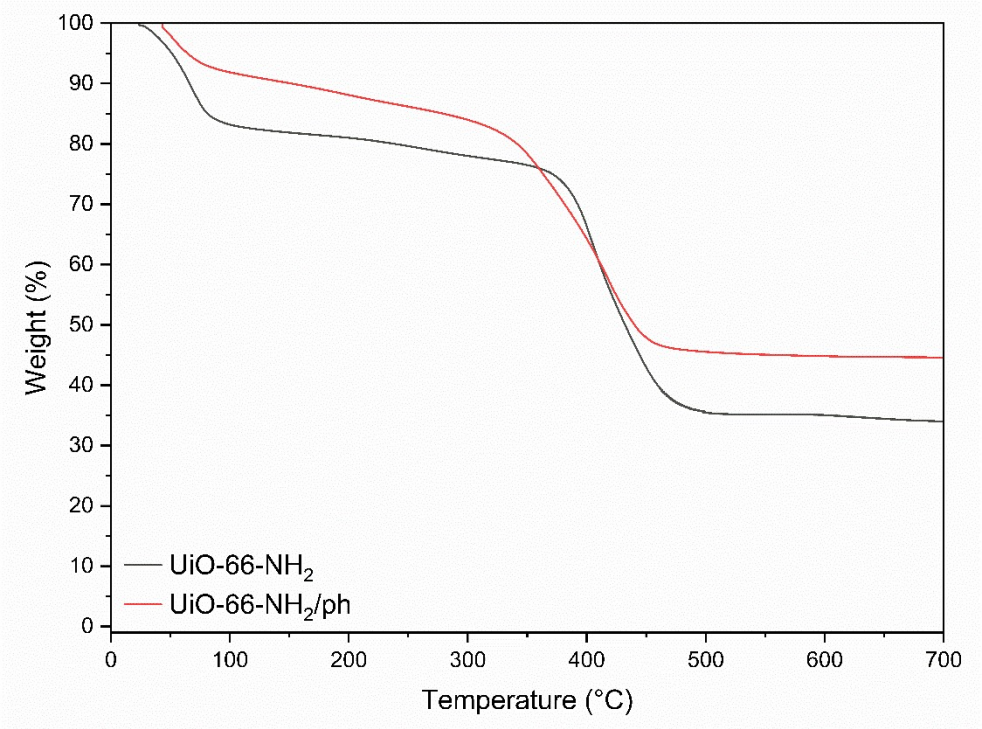

Figure S23: TGA decomposition curves of UiO-66-NH_2 (black) and UiO-66-NH_2/ph (red).

Gas Sorption Properties

Table S4: Properties of pristine UiO-66-NH_2 and its modified derivatives.

Material	**BET Surface Area (m^2g^{-1})**	**CO_2 Uptake at 1000 mbar (mmol g^{-1})**	**Pore Volume (cm^3 g^{-1})**	**Pore Diameter (Å)**	**Enthalpy of Adsorption (ΔH_{ads}^0) (kJ mol^{-1})**
UiO-66-NH_2	1,054 ± 19	1.99	0.44	16.52	27.47
UiO-66-NH_2/DC	465 ± 6	1.70	0.19	16.73	27.92
UiO-66-NH_2/Eu	759 ± 9	2.19	0.30	15.33	29.12
UiO-66-NH_2/PA	776 ± 9	1.54	0.31	15.85	28.21
UiO-66-NH_2/ph	66 ± 1	0.61	0.03	17.73	31.57

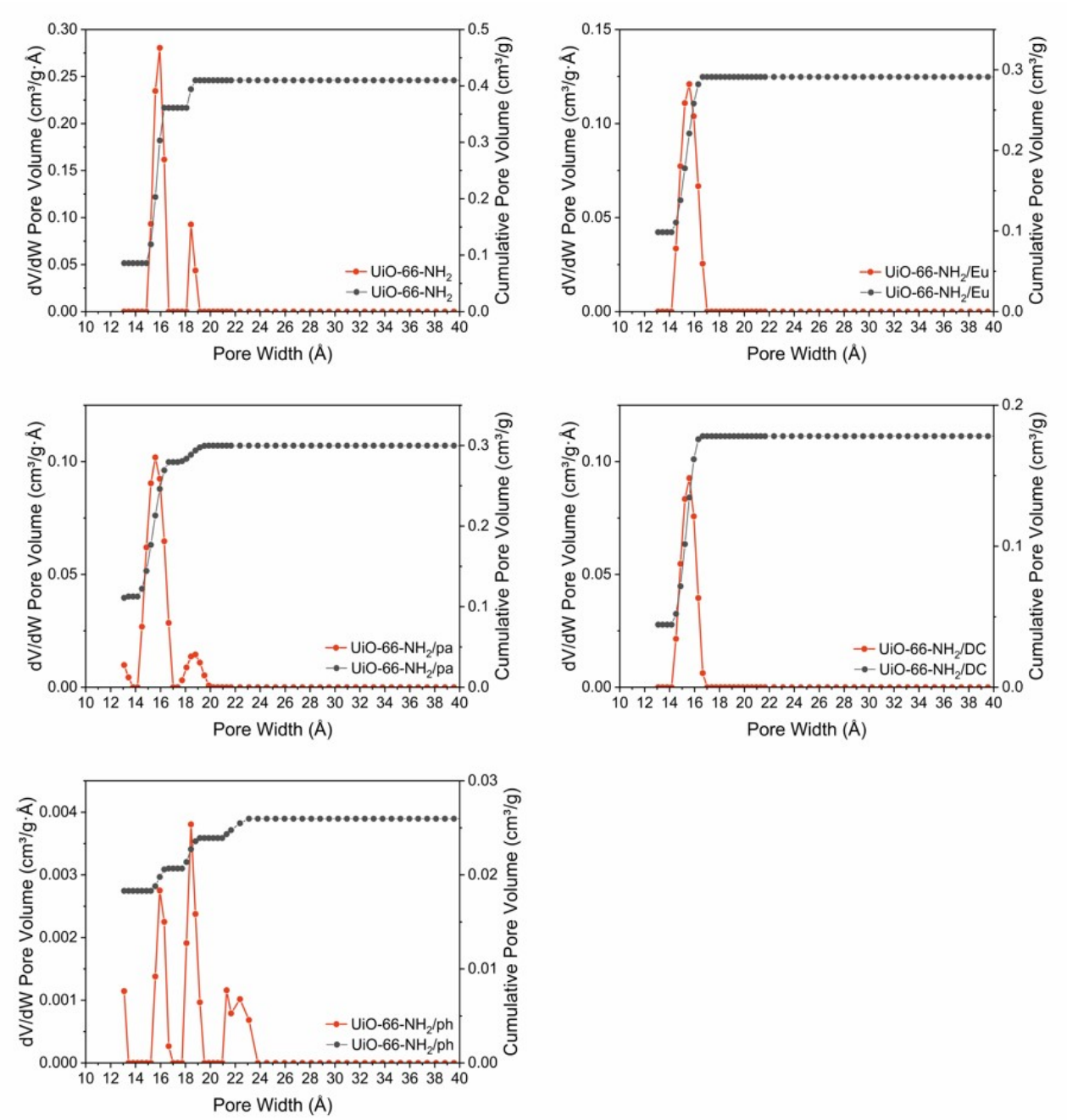

Figure S24: Pore size distribution of UiO-66-NH_2 (top left), UiO-66-NH_2/Eu (top right), UiO-66-NH_2/PA (middle left), UiO-66-NH_2/DC (middle right) and UiO-66-NH_2/ph (bottom right). Black lines represent the cumulative pore volume and red lines represent the pore width.

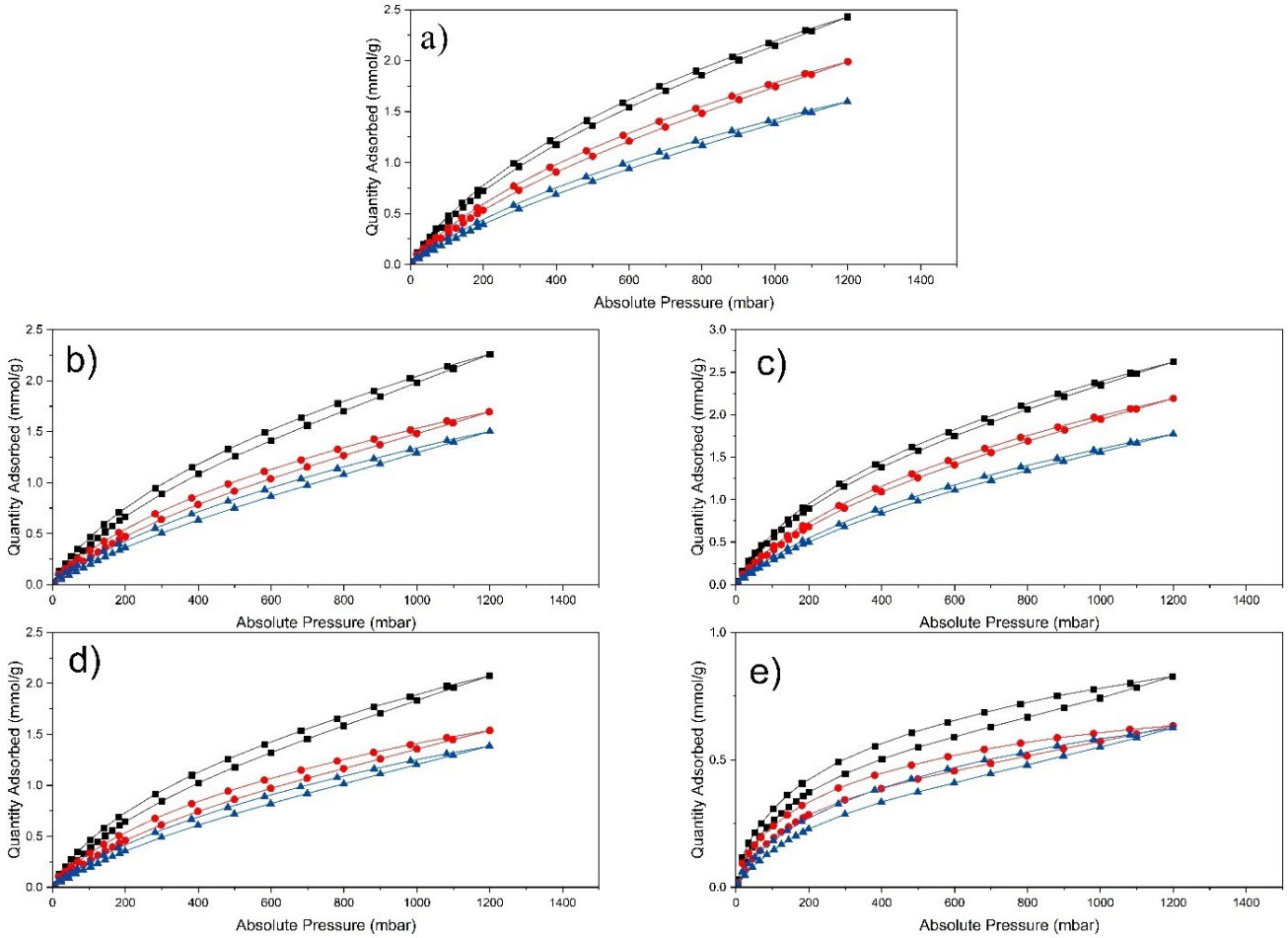

Figure S25: Isosteric heat of adsorption measurements performed at 288 K (black), 298 K (red) and 308 K (blue) on **(a)** UiO-66-NH_2 **(b)** UiO-66-NH_2/DC **(c)** UiO-66-NH_2/Eu **(d)** UiO-66-NH_2/PA **(e)** UiO-66-NH_2/ph.

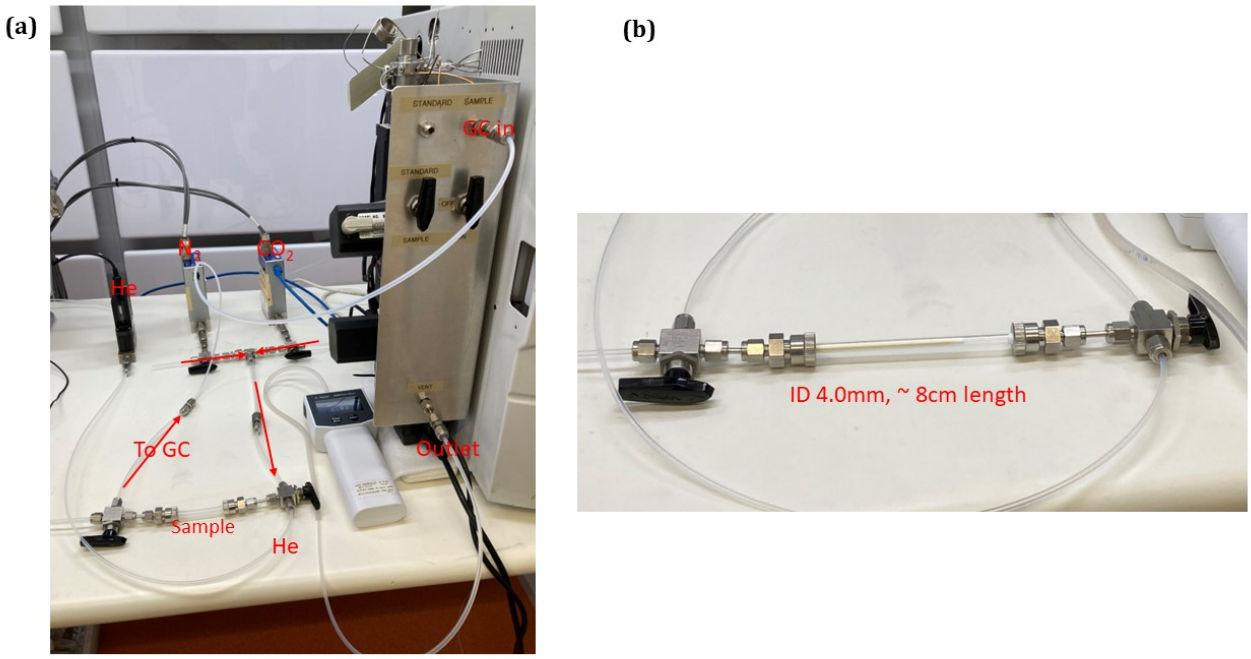

Figure S26: (a) Set-up of breakthrough rig and **(b)** the size of the column used.

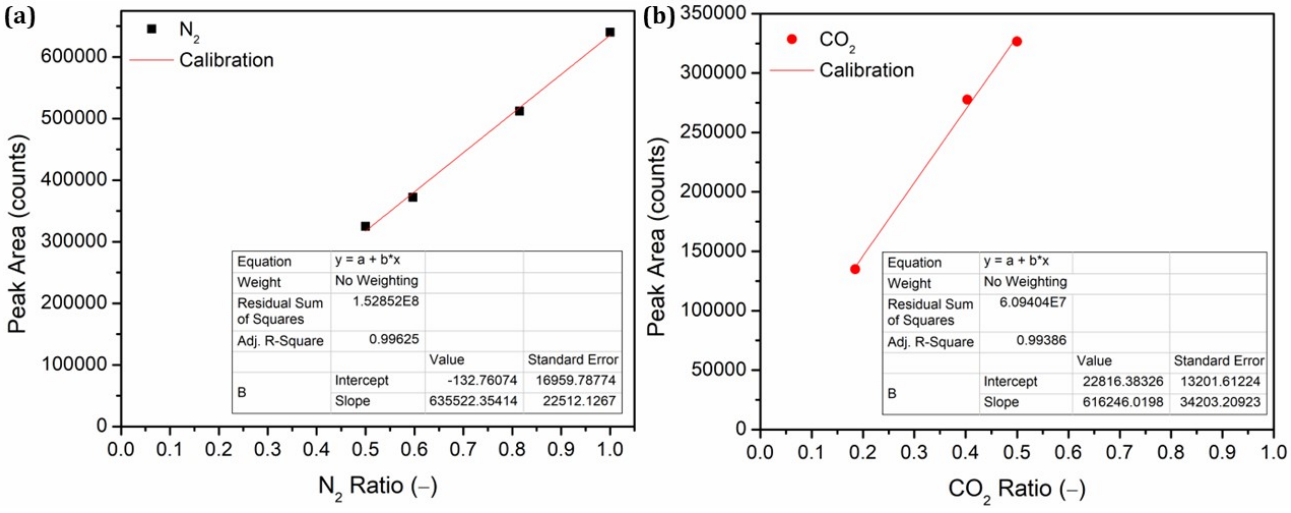

Figure S27: Calibration curves for **(a)** N_2 and **(b)** CO_2.

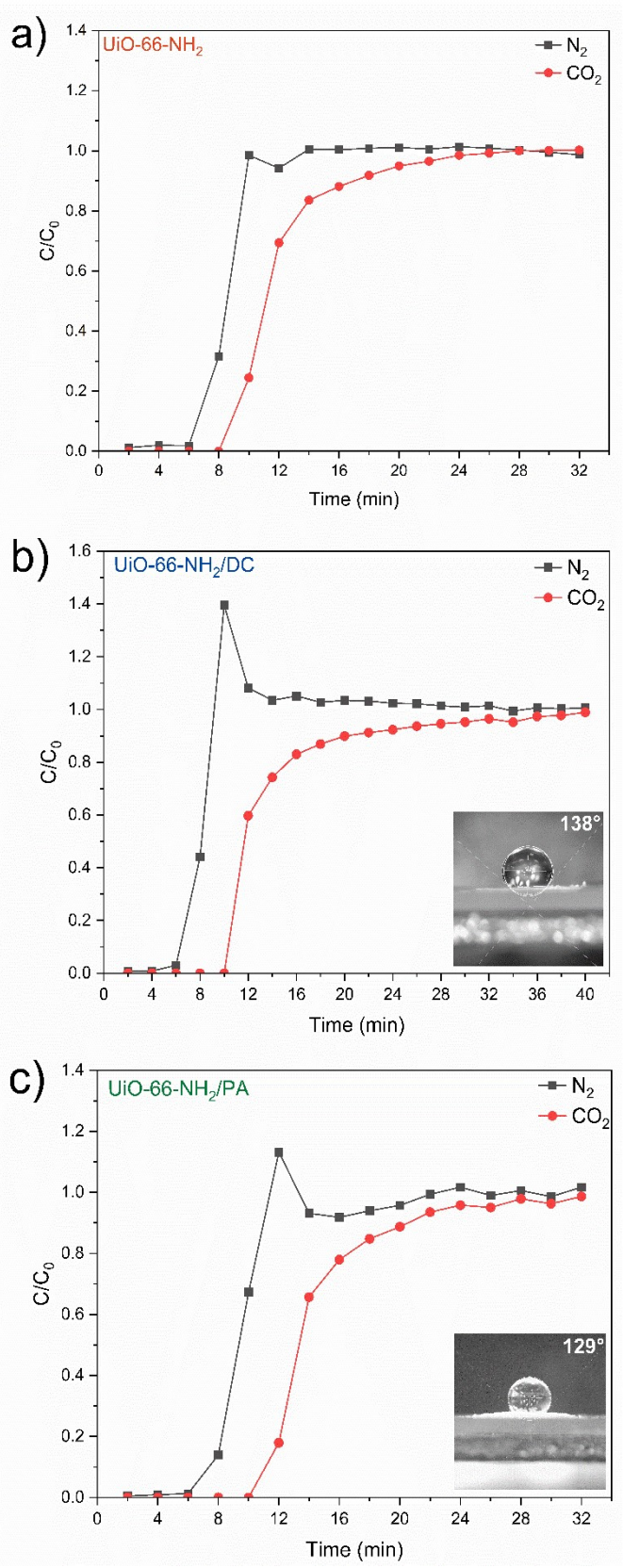

Figure S28: N_2 (black) and CO_2 (red) breakthrough curves for **(a)** UiO-66-NH_2 **(b)** UiO-66-NH_2/DC and **(c)** UiO-66-NH_2/PA at 298 K. N_2 CO_2 breakthrough are shown in black and red, respectively. Inset: water contact Angle measurements for **(b)** UiO-66-NH_2/DC and **(c)** UiO-66-NH_2/PA.

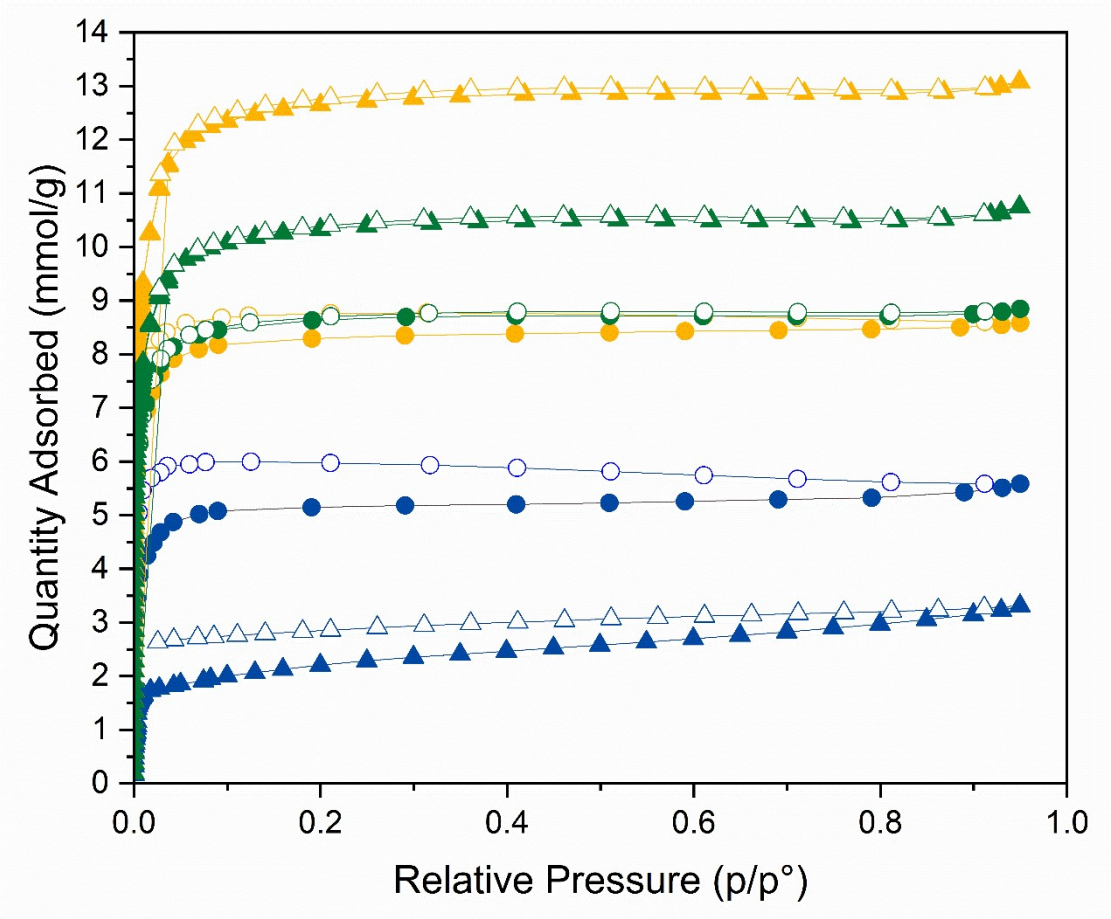

Figure S29: N_2 gas sorption measurements performed at 77 K for UiO-66-NH_2/DC (blue), UiO-66-NH_2/Eu (yellow) and UiO-66-NH_2/PA (green) prior to (circles), and following (triangles), wetting**.** Adsorption and desorption isotherms measured on pristine samples are denoted by filled and hollow symbols, respectively. Adsorption and desorption isotherms measured on wetted samples are denoted by horizontal and vertical half-filled symbols, respectively.

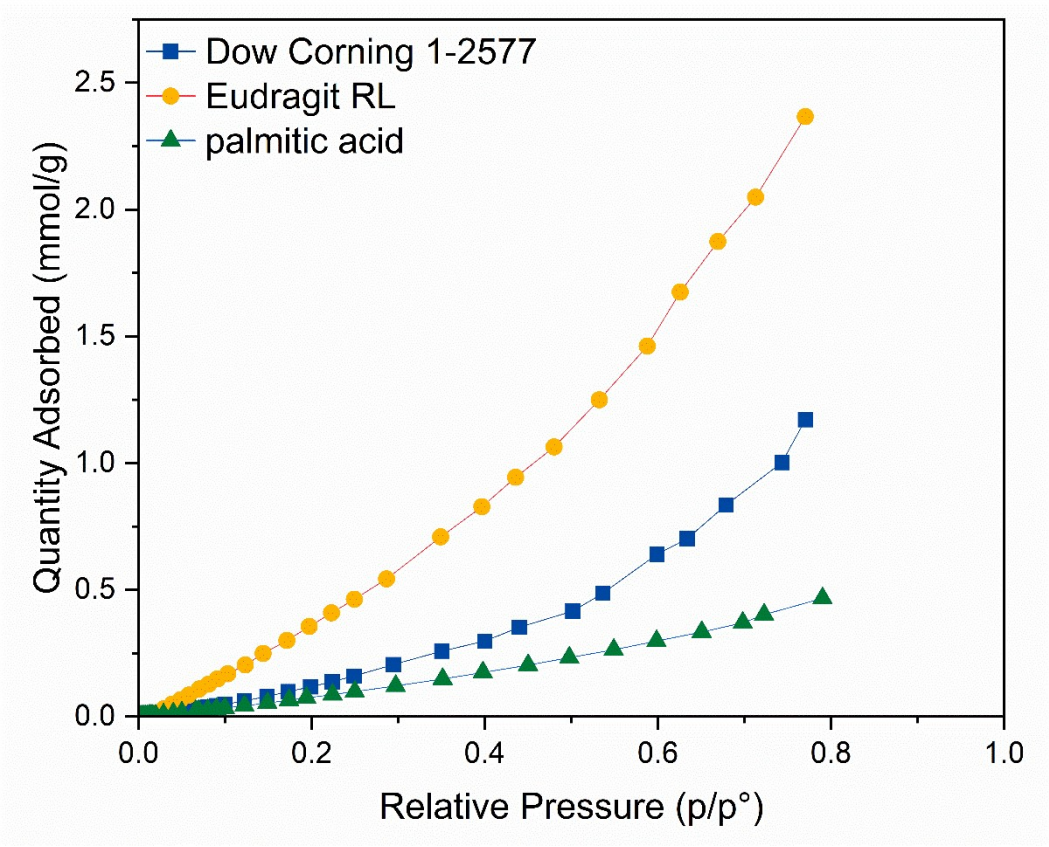

Figure S30: H_2O adsorption isotherms at 298 K of pristine Dow Corning 1-2577 (blue), Eudragit RL ® (yellow) and palmitic acid (green) coating material.

References

1. G. Eggert, *Herit. Sci.*, 2022, **10**, 54.
2. S. Brunauer, P. H. Emmett and E. Teller, *J. Am. Chem. Soc.*, 1938, **60**, 309-319.
3. D. Ambrose and I. J. Lawrenson, *J. Chem. Thermodyn,*, 1972, **4**, 755-761.
4. C. A. Schneider, W. S. Rasband and K. W. Eliceiri, *Nat Methods*, 2012, **9**, 671-675.
5. H. X. Luo, F. W. Cheng, L. Huelsenbeck and N. Smith, *J. Environ. Chem. Eng.*, 2021, **9**, 105159.
6. G. Kaur, J. Grewal, K. Jyoti, U. K. Jain, R. Chandra and J. Madan, in *Drug Targeting and Stimuli Sensitive Drug Delivery Systems*, ed. A. M. Grumezescu, William Andrew Publishing, 2018, pp. 567-626.
7. T. J. Shaffner and R. D. V. Veld, *J. Phys. E Sci. Instrum.*, 1971, **4**, 633-637.
8. B. Yuan, G. Gou, T. Fan, M. Liu, Y. Ma, R. Matsuda and L. Li, *Angew. Chem. Int. Ed.*, 2022, **61**, e202204568.
9. Y. Toivola, S. Kim, R. F. Cook, K. Char, J. K. Lee, D. Y. Yoon, H. W. Rhee, S. Y. Kim and M. Y. Jin, *J. Electrochem. Soc.*, 2004, **151**, F45-F53.
10. D. Sun, P. R. Adiyala, S. J. Yim and D. P. Kim, *Angew. Chem. Int. Ed.*, 2019, **58**, 7405-7409.
11. C. Fang, C. L. Lu, M. H. Liu, Y. L. Zhu, Y. Fu and B. L. Lin, *ACS Catal.*, 2016, **6**, 7876-7881.
12. Y. L. Hsiao and R. M. Waymouth, *J. Am. Chem. Soc.*, 1994, **116**, 9779-9780.